Exciton mobility control through sub-Å packing modifications in molecular crystals

Nicholas J. Hestand, Roel Tempelaar, Jasper Knoester, Thomas L. C. Jansen, and Frank C. Spano

Phys. Rev. B **91**, 195315 — Published 18 May 2015

DOI: 10.1103/PhysRevB.91.195315

Exciton Mobility Control through sub-Angstrom Packing Modifications in Molecular Crystals

Nicholas J. Hestand[1], Roel Tempelaar[2], Jasper Knoester[2], Thomas L. C. Jansen[2], Frank C. Spano[1*]

[1]Department of Chemistry, Temple University, Philadelphia, PA 19122, United States
[2]Zernike Institute for Advanced Materials, University of Groningen, Nijenborgh 4, 9747 AG Groningen, The Netherlands

Abstract: Exciton mobility in π-stacks of organic chromophores is shown to be highly sensitive to the interference between long-range Coulomb coupling and a short-range coupling due to wave function overlap. A destructive interference which leads to a compromised exciton bandwidth can be converted to constructive interference (and an enhanced bandwidth) upon sub-Å transverse displacements between neighboring chromophores. The feasibility of the control scheme is demonstrated theoretically on a derivative of terrylene, where the exciton is essentially immobile despite strong Coulombic coupling. A transverse slip of only 0.5 Å along either the short or long molecular axis boosts the exciton velocity to 2×10^4 m/sec. Changes in the mobility are correlated to changes in the absorption spectrum, allowing the latter to be used as a screen for high-mobility aggregates.

I. Introduction

Optimizing energy and charge transport is a crucial element in the design of efficient organic-based photovoltaic and light-emitting devices. Transport in such devices is usually attributed to incoherent hopping[1], although there is increasing evidence of a subpicosecond coherent contribution.[2-5] The mobility of singlet excitons is derived mainly from the Coulombic coupling between chromophores, consistent with the fundamental excitations being Frenkel-type excitons where the electron and hole remain bound to the parent molecule. However, in tightly-packed π-stacked organic crystals, such as those corresponding to a multitude of perylene-based dyes[6-8], the close proximity of neighboring molecules leads to significant charge transfer (CT) between chromophores through the spatial overlap of their frontier molecular orbitals. It is well known that the electron and hole bandwidths, as well as the optical bandgap in perylene dyes, are very sensitive to sub-Å shifts ("slips") in the relative orientations of neighboring molecules, leading to the remarkable range of colors displayed by such dyes in the crystalline phase. This effect, known as crystallochromy[9-13], is attributed to the changing registry of the frontier

molecular orbitals of nearest neighbor molecules. Small changes in the slip-stacking distance are also thought to play a strong role in the efficiency of singlet exciton fission.[14-16]

In a recent work,[17] the unusual photophysical properties of 7,8,15,16-tetraazaterrylene (TAT) nanopillars grown on silica substrates[18] were explored, showing that the two-band nature of its crystal-phase absorption spectrum[18, 19] can be understood as an interference between Coulombic coupling, which promotes H-aggregate behavior (blue-shifted features), and CT-mediated coupling, which promotes J-aggregate behavior[20] (red-shifted features). The interference was also shown to lead to a significant reduction in the exciton bandwidth, suggesting a coincident reduction in the exciton mobility. Interestingly, the TAT nanopillars show structured exciton emission,[19] so that exciton mobility is not inhibited by excimer trap formation, as it is in similarly packed perylene crystals.[8, 21] Even more recently, the same interference effect was employed to explain dynamic fluctuations in the net excitonic coupling induced by thermal motions of the nuclei in anthracene and polyaromatic hydrocarbons.[22] In the present manuscript, we investigate exciton dynamics in TAT stacks and find a dramatic dependence of the exciton velocity on small (sub-Å) slips of one TAT molecule relative to its neighbor. Hence, it should be possible to exploit this dynamic crystallochromy-like effect to control the rate of energy transfer in organic materials.

II. Theory

The nature of interference between the long-range Coulombic and short-range CT-mediated couplings can be appreciated within the framework of the electronic Hamiltonian,

$$\hat{H}_{el} = \sum_{m,n}(J_{m,n} - U\delta_{m,n})B_m^\dagger B_n + \sum_n [t_e c_n^\dagger c_{n+1} + t_h d_n^\dagger d_{n+1} + h.c.] - \sum_{n,s\neq 0} V_{CT}(s) c_n^\dagger c_n d_{n+s}^\dagger d_{n+s} \qquad (1)$$

where we assume a subspace consisting of a single electron and a single hole. For the *n*th chromophore, $c_n^\dagger(c_n)$ creates (annihilates) an electron in the LUMO orbital, $d_n^\dagger(d_n)$ creates (annihilates) a hole in the HOMO orbital, and $B_n^\dagger$ $(= c_n^\dagger d_n^\dagger)$ and B_n, creates and annihilates a local Frenkel excitation, respectively. The first term in $\hat{H}$ accounts for energy transfer between the *n*th and *m*th chromophores, occurring directly via the Coulombic coupling, $J_{m,n}$. The term also includes the local exciton binding energy *U*. Charge transfer is mediated by the electron (t_e) and

hole (t_h) transfer integrals appearing in the second summation. Such terms also couple the locally excited Frenkel excitons to CT excitons. The latter consist of anion-cation pairs; for charges separated by $|s|d$, where d is the distance between nearest-neighbor (n.n.) chromophores, the Coulomb binding energy is, $V_{CT}(s) = e^2 / (4\pi\varepsilon_0\varepsilon_R \,|\, s \,|\, d)$

In order to obtain quantitative agreement for the TAT absorption spectrum one needs to include vibronic coupling involving the prominent 1200 cm^{-1} intramolecular stretching mode that is responsible for the pronounced vibronic progressions observed in the absorption and PL spectra.[18, 19] We use a Holstein-style Hamiltonian to account for the exciton-vibrational coupling involving this mode, so that the complete Hamiltonian is written as,[23]

$$\begin{aligned}\hat{H} = \hat{H}_{el} &+ \hbar\omega_{vib}\sum_n b_n^\dagger b_n + \hbar\omega_{vib}\sum_n \{\lambda(b_n^\dagger + b_n) + \lambda^2\} B_n^\dagger B_n \\ &+ \hbar\omega_{vib}\sum_{n,s\neq 0} \{\lambda_-(b_n^\dagger + b_n) + \lambda_+(b_{n+s}^\dagger + b_{n+s}) + \lambda_-{}^2 + \lambda_+{}^2)\} c_n^\dagger c_n d_{n+s}^\dagger d_{n+s} \\ &+ U + \omega_{0-0} + \Delta_{0-0}\end{aligned} \tag{2}$$

In Eq. (2), $b_n^\dagger(b_n)$ creates (annihilates) a vibrational quantum on molecule n with energy $\hbar\omega_{vib}$ (=1200 cm^{-1}) corresponding to the intramolecular stretching mode. The nuclear potential well of this mode is assumed harmonic and characterized by a shifted equilibrium geometry when the molecule is in an excited or ionic state. The corresponding relaxation energy of an exciton is given by $\hbar\omega_{vib}\lambda^2$ where λ^2 defines the dimensionless Huang-Rhys (HR) parameter. For the anionic and cationic states the respective relaxation energies are $\hbar\omega_{vib}\lambda_-^2$ and $\hbar\omega_{vib}\lambda_+^2$, with the associated HR factors given by, λ_-^2 and λ_+^2. The final three terms of the Hamiltonian in Eq.(2) collectively define the molecular transition energy between the ground and excited state; ω_{0-0} is the excitation energy of a monomer in solution and Δ_{0-0} is the solution-to-crystal energetic shift. Note the addition of U ensures that the transition energy in the limit of single chromophores is equal to $\omega_{0-0} + \Delta_{0-0}$.

In addition to Coulomb coupling, energy transfer can be accomplished via CT-mediated transfer of a single electron and a single hole; in the limit that the diabatic Frenkel band is energetically well-separated from the charge transfer band (by >> $|t_e|,|t_h|,\hbar\omega_{vib}$) , application of

second order perturbation theory yields an effective Frenkel exciton Hamiltonian which replaces the electronic part in Eq.(1)[20],

$$\hat{H}_{eff} = \sum_{n} (\Delta_{SR} - U) B_n^{\dagger} B_n + \sum_{m,n} (J_{m,n} + J_{SR}\delta_{m,n\pm 1}) B_m^{\dagger} B_n \tag{3}$$

where,

$$J_{SR} = -\frac{2t_e t_h}{U - V_{CT}(1)} \tag{4}$$

is the effective short-range coupling mediated by a virtual CT state[20] , and

$$\Delta_{SR} = -\frac{2(t_e^{\,2} + t_h^{\,2})}{U - V_{CT}(1)} \tag{5}$$

is the second-order energy level shift. The effective Hamiltonian shows that the short-range coupling, J_{SR} , interferes directly with the n.n. Coulombic coupling.[24-26] For TAT, our calculations reveal a screened n.n. Coulomb coupling of approximately 300-400 cm^{-1} which is compensated by a short-range coupling of comparable magnitude but opposite sign.[17] Such aggregates were referred to as HJ-aggregates because the positive Coulomb coupling promotes H-like photophysical behavior, while the negative CT-mediated coupling promotes J-like behavior. While the concept of competing short- (J_{SR}) and long-range (J_{nm}) coupling is rigorous only for the (second order) electronic Hamiltonian, it nevertheless remains a valid qualitative description for the behavior derived from the more complex vibronic Hamiltonian parameterized for TAT in Eq. (2); indeed, when the full Hamiltonian was analyzed, it was shown that the exciton bandwidth is narrowed by a factor of three when CT coupling is activated. The question naturally arises as

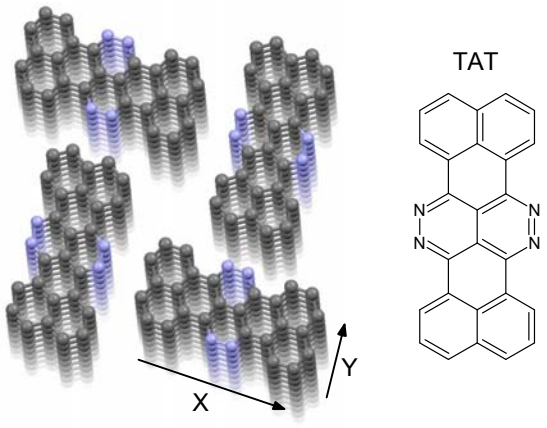

Figure 1. The crystal structure of TAT nanopillars, [18] viewed down the stacking axis, is shown on the left. Here X and Y denote the long and short molecular axes respectively. The chemical structure of TAT is shown on the right.

to the sensitivity of the bandwidth reduction to sub-Å slips between neighboring chromophores: is it possible that such slips can induce a sign change in J_{SR} , but not in the long-range Coulomb

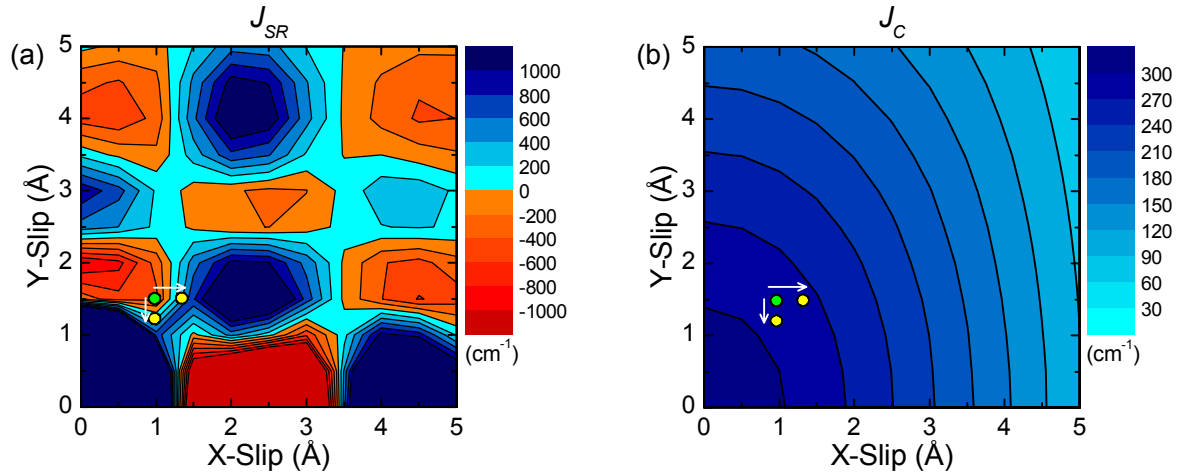

Figure 2. (a) The calculated short-range coupling J_{SR} and (b) the nearest-neighbor Coulomb coupling J_C as a function of the transverse displacement in a cofacial TAT dimer. The origin indicates the eclipsed geometry. Blue regions indicate a positive coupling and hence H-aggregation while red regions indicate a negative coupling and J-aggregation. The natural geometry of TAT (green dot) lies in a red region of the short range coupling and a blue region of the long-range (Coulomb) coupling, making TAT an HJ-aggregate. A slight shift along either molecular axis (yellow dots) has virtually no effect on the Coulomb coupling but leads to a sign change of the short range coupling, transforming TAT into a HH-aggregate with enhanced exciton transport properties. The transfer integrals t_e and t_h are found from the dimer energy splitting method where the *ab-initio* calculations set the intermolecular stacking distance to 3.3 Å and employ the B3LYP functional coupled with the 6-31G(d) basis set. J_{SR} is subsequently evaluated using Eq.(4) with $U - V_{CT}(1)$ = 1209 cm^{-1} (see Tables S.1 and S.2 for TAT parameters). The Coulomb couplings were evaluated using the transition-charge method [28,29] and subsequently scaled by the procedure outlined in Ref. [17].

couplings? If so, then the resulting *constructive* interference between short- and long-range couplings may create an enhanced excitation transfer rate with desirable properties for photovoltaic devices.

III. Spatial Dependence of the Couplings

Fig. 2a shows how sensitive J_{SR}, evaluated from Eq.(4), is to a transverse displacement between n.n. chromophores in a cofacial TAT dimer, with t_e and t_h computed using DFT with the B3LYP functional. The origin corresponds to a perfectly eclipsed orientation with cofacial separation, d= 3.3 Å, while the X and Y dimensions refer to displacements between neighboring molecules along the long and short molecular axis, respectively (see Fig. 1). The green dot indicates the relative orientation for neighboring molecules in a TAT π-stack as determined from x-ray analysis.[18] Its placement in the red region indicates short-range J-like behavior, i.e. $J_{SR} < 0$ (since $U - V_{CT}(1) > 0$ [27]). The figure shows that sub-Å slips can result in a dramatic change in

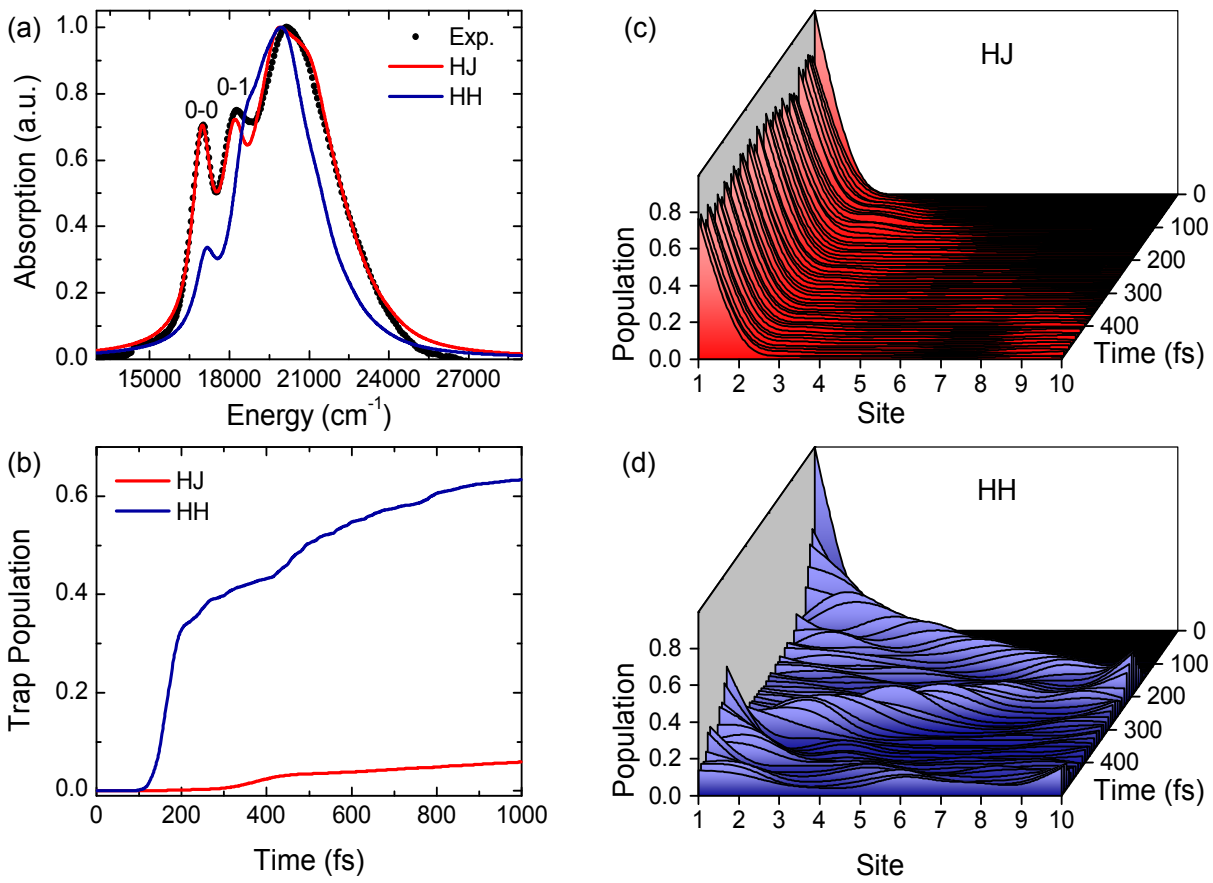

Figure 3. Calculated optical and dynamical properties of a TAT π-stack, which behaves as an HJ-aggregate, and a hypothetical π-stack obtained by reversing the sign of t_e (HH-aggregate). (a) The calculated TAT absorption spectrum (red) is compared to the experimental nanopillar spectrum from Ref. 17. Also shown is the HH aggregate spectrum (blue). The HH spectrum shows enhanced H-like behavior as the 0-0/0-1 peak ratio is suppressed due to a redistribution of oscillator strength to higher vibronic peaks. (b) (c) and (d) show the evolution of the wave function for a π-stack containing 10 molecules when initially the first molecule is excited. (b) The amount of population that has accumulated in the trap at the end of the chain as a function of time. In the HJ aggregate, the excitation cannot efficiently reach the end of the chain leading to a slow buildup of population in the trapping state, however for the HH aggregate, the exciton moves swiftly across the chain so that the excitation reaches the trap quickly. (c) and (d) show the exciton populations at each site on the chain for the HJ and HH aggregates with data points at 10 fs intervals. The HJ aggregate shows essentially zero movement of the exciton while the HH aggregate moves rapidly across the chain. Parameters for these calculations are reported in Tables S.1 and S.2.

both the sign and magnitude of the product $t_e t_h$. The two yellow dots separated from the green dot by < 0.5 Å indicate orientations in which the sign of J_{SR} becomes positive but with a magnitude unchanged from that of TAT. We have further established that the Coulombic coupling, as evaluated using atomic transition densities[28, 29], changes by less than 3% over the same displacement; Fig. 2b shows that the n.n. Coulomb coupling does not change sign over the entire range of slip displacements shown. Hence, small slip displacements can readily change the TAT HJ-aggregate into an HH-aggregate, with an anticipated marked increase in exciton mobility, as will be established below.

IV. Disorder-free TAT aggregates

To accurately assess the impact of just a sign change in J_{SR} on photophysical properties we analyzed exciton dynamics in disorder-free TAT π-stacks using the complete vibronic Hamiltonian in Eq. (2). Fig. 3a shows the simulated absorption spectrum of TAT plotted against the measured spectrum from Ref. [17], using a phenomenological Lorentzian line broadening. The two-band spectrum consists of red-shifted and blue-shifted features relative to the monomer absorption peak at approximately 18,000 cm^{-1} (not shown).[17] The spectrum can be understood in terms of an HJ-aggregate in which the two coupling sources destructively interfere, consistent with where TAT appears in Fig. 2 (green dot). Also shown in Fig. 3a is the spectrum obtained when just the sign of t_e is changed (corresponding to a yellow dot in Fig. 2), thereby changing the destructive interference into a constructive one, i.e. turning the TAT HJ-aggregate into a hypothetical HH-aggregate. The spectrum shows all of the classic H-like features[30, 31], most notably a significant drop in the 0-0/0-1 vibronic intensity ratio and an overall blue-shift relative to the solution spectrum (see Ref.[17]).

We next considered how the exciton dynamics responds to a change in the sign of t_e. To accomplish this we chose an initial condition in which the first chromophore in a π-stack containing ten chromophores is vibronically excited to the S_1 state with no vibrational quanta in the shifted (S_1) nuclear potential. Subsequent time evolution was determined by solving the Schrödinger equation using the complete vibronic Hamiltonian in Eq. (2) with the electronic Hamiltonian in Eq.(1). Fig. 3c shows how the expectation value of the n-dependent probability density, $\left\langle B_n^{\dagger} B_n \right\rangle$ evolves with time for a TAT π-stack using the same parameters which best reproduced the HJ absorption spectrum in Fig. 3a. As is immediately obvious the exciton remains practically pinned on the first chromophore for the better part of a picosecond, a result of the aforementioned destructive interference between short- and long-range couplings.

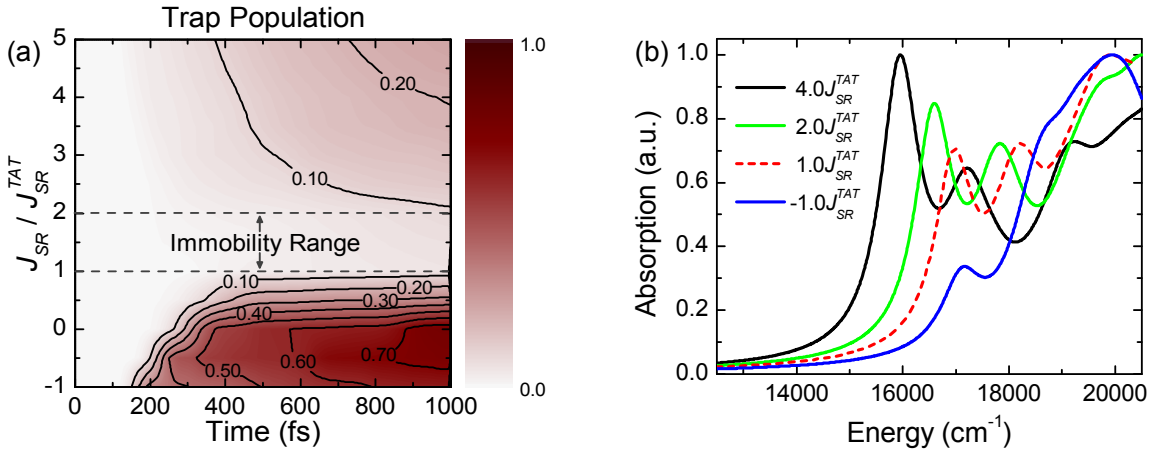

Figure 4 (a) Contour plot of the trap population as a function of time over a range of J_{SR} values using the Hamiltonian in Eq. (2) with $\hat{H}_{el}$ from Eq.(1). The parameters for the Hamiltonian are identical to those corresponding to a TAT HJ-aggregate in Fig. 3, with the exception of t_e and t_h. The latter were taken to be the TAT values (respectively, 435 and 402 cm^{-1}) multiplied by a scaling factor $\sqrt{q}$ so that the corresponding short-range coupling in Eq. (4) is scaled by q, i.e., $J_{SR} = qJ_{SR}^{TAT}$ with $J_{SR}^{TAT} = -290\ cm^{-1}$. To obtain the negative scaling, $J_{SR} = -qJ_{SR}^{TAT}$, t_e was additionally multiplied by -1. (b) Calculated absorption spectra for a π-stack containing 20 chromophores.

Fig. 3d shows the impact of changing just the sign of t_e on the exciton's motion, an effect accomplished by a < 0.5 Å slip from the green to yellow dot in Fig. 2. The corresponding change in exciton mobility is quite dramatic - the exciton is now able to traverse the length of the stack in less than 200 fs, which amounts to a velocity of approximately 2×10^4 m/sec. The enhanced mobility is essentially due to the constructive interference between short- and long-range coupling. We have further shown that if the short-range coupling in the TAT HJ-aggregate was simply set to zero, by taking either t_e or t_h to zero, or by greatly increasing $U - V_{CT}(1)$, the exciton regains mobility and the aggregate reduces to a conventional Kasha *H*-aggregate[32] (see Fig. S.1).

A quantitative measure of the efficiency of excitation transfer in the HJ and HH TAT aggregates is shown in Fig. 3b. Here, the tenth chromophore was considered a trap state[33] whose population represents the amount of excitation that has traversed the length of the chain at a specific time. Upon propagation of the quantum wave function this site was excluded from the system Hamiltonian, and instead, population at site 9 ($< B_9^\dagger B_9 >$) was transferred to the trap site at a rate of $0.15 < B_9^\dagger B_9 >$ fs^{-1}, a reasonable value to compare the transfer efficiencies for the HJ and HH-aggregates. Fig. 3b shows how the trap population builds up over time for the two

aggregate types. Again, a sign change in the short-range coupling has a dramatic impact on the exciton transfer rate; after 1 ps the HH-aggregate is found to transport approximately 10 times more population than the HJ variant.

In order to appreciate the robustness of the destructive interference in HJ aggregates we evaluated the evolution of the exciton trap population over a range of J_{SR} values (leaving the Coulombic coupling unchanged). The results, shown in the contour plot of Fig. 4a, cover a range of J_{SR} values from $5J_{SR}^{\mathrm{TAT}}$ to $-J_{SR}^{\mathrm{TAT}}$, where J_{SR}^{TAT} ($= -290$ cm^{-1}) is the short-range coupling corresponding to the (TAT) HJ-aggregate simulations of Fig. 3. Fig. 4b shows representative absorption spectra. When $J_{SR} = -J_{SR}^{\mathrm{TAT}}$, the (positive) short-range coupling reinforces the positive Coulombic couplings leading to high exciton mobility and a small 0-0/0-1 peak ratio, indicative of H-aggregation. As J_{SR} decreases through zero and becomes increasingly more *negative* the absorption spectrum displays more J-like character: the absorption origin increasingly red-shifts and the 0-0/0-1 intensity ratio increases. At the same time the exciton becomes increasingly less mobile, reflective of a more efficient destructive interference between the long- and short-range couplings. At the TAT point ($J_{SR} = J_{SR}^{\mathrm{TAT}}$) the cancellation of the two coupling sources is quite efficient, as evidenced by a 0-0/0-1 ratio which is about equal to the monomer value (≈ 1, see Ref.[17]). Interestingly, making J_{SR} even more negative has little effect on the mobility when $J_{SR}^{\mathrm{TAT}} > J_{SR} > 2J_{SR}^{\mathrm{TAT}}$. However, once outside this range the mobility begins to recover, being driven by the dominating influence of the short-range coupling. Overall, Fig. 4a shows that the low-mobility region of efficient destructive interference extends over a wide range of short-range couplings; for J_{SR} in the range $J_{SR}^{\mathrm{TAT}} > J_{SR} > 2J_{SR}^{\mathrm{TAT}}$ the exciton is practically immobile.

V. Effects of Bath Fluctuations

The analyses presented so far were based on TAT aggregates free from any impurities, where the excitation was allowed to perform ballistic motion while perfectly maintaining its phase. However, the line broadening observed in absorption spectroscopy of TAT is considerable, suggesting the presence of strong bath fluctuations that impact excitation mobility through scattering events. As shown in Fig. 3a, the experimental absorption band can be reproduced accurately using a Lorentzian line shape.[17] Nevertheless, in order to evaluate the exciton mobility under realistic conditions, the microscopic processes underlying spectral line broadening must be

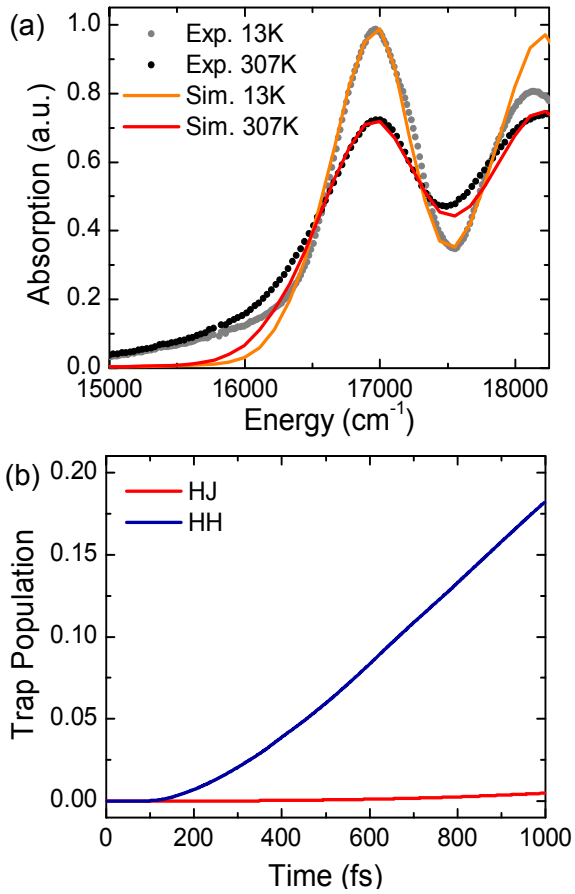

Figure 5. (a) The temperature dependent broadening of the 0-0 absorption peak is used to determine the relative contributions of static and dynamic disorder in TAT. (b) The population of the trapping site for the disordered HJ and HH aggregate, showing that the contrasting behaviors of constructive and destructive couplings are robust against disorder and dephasing, and in fact may even be enhanced by such effects.

accounted for. Fig. 5 demonstrates the robustness of the aforementioned results when the HJ and HH-aggregates are coupled to a bath so that dephasing becomes activated. Rather than attempting to rigorously account for the multiplicity of bath modes involved in TAT, we considered a qualitative bath description, employing the simplest possible model that is consistent with the experimental data. The applied model distinguishes between two components affecting the site transition energies: Gaussian static disorder, and thermal fluctuations described through the over-damped Brownian oscillator model (see Supplemental Section II for details).[34] The latter corresponds to Gaussian-stochastic energy trajectories with a standard deviation that scales as $T^{1/2}$. The relative contributions of the two bath components is derived by fitting calculated absorption spectra to temperature-dependent measurements, as shown in Fig. 5a. This fitting procedure is limited to the lowest-energy absorption band, since the higher-energy vibronic replicas likely experience additional broadening due to a variety of closely-spaced vibrational modes represented by an effective 1200 cm^{-1} vibration.[3]

Shown in Fig. 5b are room temperature calculations of the trap population. As expected, inclusion of dephasing strongly impacts the excitation dynamics, washing out the coherence and limiting the transfer speed. The contrast in excitation mobility between the HJ and HH aggregate comes out even more pronounced under such realistic conditions. After 1 ps, the trap population in the HH aggregate has grown to become about 35 times the value reached for the HJ analogue. This surprising behavior can be understood by considering that for two molecules the same

deviation from resonance, as quantified by the difference of the two on-site transition energies, will have a stronger localizing effect on weakly coupled molecules (HJ) in which the total coupling is compromised due to destructive interference, than on strongly coupled ones (HH) in which the couplings reinforce each other.

VI. Conclusion

The results presented here offer a design strategy for improving energy transport in organic materials by engineering the crystal packing structure so that the short-range and long-range couplings constructively interfere. Unlike the long-range Coulombic coupling, the CT-mediated short-range coupling is hypersensitive to sub-Å slips between neighboring molecules within a π-stack. Such displacements are tunable through chemical modification; for example, a recent report shows that slip distances along the long molecular axis correlate to the bulkiness of the terminally-substituted groups in a series of perylene derivatives.[35] Sub-Å displacements may also be induced through lattice strain. Using a solution-shearing technique, Giri et. al.[36] reduced the π-stacking distance in TIPS pentacene by approximately 0.2 Å, creating an almost six-fold increase in the hole mobility due to enhanced HOMO-HOMO overlap.

We have also shown a strong correlation between the absorption spectral line shape and the exciton mobility (see Fig. 4), allowing one to potentially use the absorption spectrum to screen for high mobility aggregates. For example, if the 0-0/0-1 ratio of vibronic oscillator strengths in the solid-phase is roughly equal to the ratio observed from unaggregated (i.e. solution-phase) molecules, then the short-range and long-range couplings are effectively cancelled, yielding a low mobility exciton. Such is the case for TAT, where the 0-0/0-1 ratio is practically unchanged upon aggregation.[17] According to Fig. 4, aggregates in which the 0-0/0-1 ratio strongly deviates from the monomer value have the highest mobilities.

Furthermore, we have shown that the concept of interfering couplings remains robust even when diagonal disorder is present in the aggregate (see Fig.5), so that interference effects should persist in real systems. In a recent report, Arago and Troisi[22] showed that thermal fluctuations in the exciton couplings in polyacene crystals, fueled mainly by the relative twisting motions between edge-to-face neighbors in a herringbone lattice, can be comparable to the mean exciton couplings. In the π-stacks of interest here the excitonic couplings would be most sensitive to

fluctuations along the slip and stacking directions induced by longitudinal and optical phonons. We speculate that there is less resistance to twisting a molecule about its long axis within a herringbone lattice than to shearing one molecule against its neighbor within a π-stack, so that the relative fluctuations in the excitonic couplings would be smaller in π-stacks compared to herringbone lattices. Although the calculations presented so far do not explicitly include off-diagonal disorder we can gauge its impact by consulting Fig. 4a. As stated earlier, the exciton (in TAT stacks) remains immobile, reflective of efficient destructive interference between the charge-mediated interactions and Coulomb interactions, for a wide range of J_{SR} values. Hence, fluctuations in J_{SR} should be reasonably well-tolerated for observing either destructive or constructive interference, even when the standard deviation approaches the mean. The remarkable resiliency of the interference effect to disorder, as well as its hypersensitivity to slip-stacking, offers a thrilling prospect for optimizing excitation transport in disordered materials.

Acknowledgements: F.C.S. is supported by the National Science Foundation (grant no. DMR-1203811).

References

1. C. J. Bardeen, Annu. Rev. Phys. Chem. **65**, 127-148 (2014).
2. L. G. Kaake, J. J. Jasieniak, R. C. Bakus, G. C. Welch, D. Moses, G. C. Bazan and A. J. Heeger, J. Am. Chem. Soc. **134** (48), 19828-19838 (2012).
3. N. Banerji, J. Mater. Chem. C **1**, 3052-3066 (2013).
4. Y. Song, S. N. Clafton, R. D. Pensack, T. W. Kee and G. D. Scholes, Nat Commun **5**, 4933 (2014).
5. S. M. Falke, C. A. Rozzi, D. Brida, M. Maiuri, M. Amato, E. Sommer, A. De Sio, A. Rubio, G. Cerullo, E. Molinari and C. Lienau, Science **344** (6187), 1001-1005 (2014).
6. F. Wurthner, Chem. Comm. (14), 1564-1579 (2004).

7. H. Langhals and W. Jona, Angewandte Chemie-International Edition **37** (7), 952-955 (1998).

8. E. A. Margulies, L. E. Shoer, S. W. Eaton and M. R. Wasielewski, Phys. Chem. Chem. Phys. **16** (43), 23735-23742 (2014).

9. P. M. Kazmaier and R. Hoffmann, J. Am. Chem. Soc. **116** (21), 9684-9691 (1994).

10. L. Gisslen and R. Scholz, Phys. Rev. B **83** (15), 155311 (2011).

11. L. Gisslen and R. Scholz, Phys. Rev. B **80** (11), 115309 (2009).

12. G. Klebe, F. Graser, E. Hädicke and J. Berndt, Acta Crystallographica Section B **45** (1), 69-77 (1989).

13. M. C. R. Delgado, E.-G. Kim, D. A. d. S. Filho and J.-L. Bredas, J. Am. Chem. Soc. **132** (10), 3375-3387 (2010).

14. L. J. Wang, Y. Olivier, O. V. Prezhdo and D. Beljonne, J. Phys. Chem. Lett. **5** (19), 3345-3353 (2014).

15. S. W. Eaton, L. E. Shoer, S. D. Karlen, S. M. Dyar, E. A. Margulies, B. S. Veldkamp, C. Ramanan, D. A. Hartzler, S. Savikhin, T. J. Marks and M. R. Wasielewski, J. Am. Chem. Soc. **135** (39), 14701-14712 (2013).

16. M. B. Smith and J. Michl, Ann. Rev. Phys. Chem. **64**, 361–386 (2013).

17. H. Yamagata, D. S. Maxwell, J. Fan, K. R. Kittilstved, A. L. Briseno, M. D. Barnes and F. C. Spano, J. Phys. Chem. C **118** (49), 28842-28854 (2014).

18. J. Fan, L. Zhang, A. L. Briseno and F. Wudl, Org. Lett. **14** (4), 1024-1026 (2012).

19. A. J. Wise, Y. Zhang, J. Fan, F. Wudl, A. L. Briseno and M. D. Barnes, Phys. Chem. Chem. Phys. **16**, 15825-15830 (2014).

20. H. Yamagata, C. M. Pochas and F. C. Spano, J. Phys. Chem. B **116**, 14494-14503 (2012).

21. A. Schubert, V. Settels, W. Liu, F. Würthner, C. Meier, R. F. Fink, S. Schindlbeck, S. Lochbrunner, B. Engels and V. Engel, J. Phys. Chem. Lett. **4** (5), 792-796 (2013).

22. J. Aragó and A. Troisi, Phys. Rev. Lett. **114** (2), 026402 (2015).

23. T. Holstein, Ann Phys **8**, 325-342 (1959).

24. R. D. Harcourt, G. D. Scholes and K. P. Ghiggino, J. Chem. Phys. **101** (12), 10521-10525 (1994).

25. G. D. Scholes, R. D. Harcourt and K. P. Ghiggino, The Journal of chemical physics **102** (24), 9574-9581 (1995).

26. R. D. Harcourt, K. P. Ghiggino, G. D. Scholes and S. Speiser, J. Chem. Phys. **105** (5), 1897-1901 (1996).

27. In TAT, one cannot reproduce the vibronic features in the measured absorption spectrum if the diabatic CT states lie energetically below the Frenkel states. If the latter were true the short-range coupling would change sign yielding an HH-aggregate with very different spectral signatures than the HJ-aggregate (see Fig. 2a).

28. J. C. Chang, J. Chem. Phys. **67** (9), 3901-3909 (1977).

29. K. A. Kistler, F. C. Spano and S. Matsika, J. Phys. Chem. B **117** (7), 2032-2044 (2013).

30. F. C. Spano, Acc. Chem. Res. **43** (3), 429-439 (2010).

31. F. C. Spano, Ann. Rev. Phys. Chem. **57**, 217-243 (2006).

32. M. Kasha, H. R. Rawls and M. A. El-Bayoumi, in *Molecular Spectroscopy* (Butterworths, London, 1965), pp. 371-392.

33. S. M. Vlaming, V. A. Malyshev and J. Knoester, J. Chem. Phys. **127** (15), 154719 (2007).

34. S. Mukamel, *Principles of Nonlinear Optical Spectroscopy*. (Oxford University Press, New York, 1995).

35. P. E. Hartnett, A. Timalsina, H. S. S. R. Matte, N. Zhou, X. Guo, W. Zhao, A. Facchetti, R. P. H. Chang, M. C. Hersam, M. R. Wasielewski and T. J. Marks, J. Am. Chem. Soc. **136** (46), 16345-16356 (2014).

36. G. Giri, E. Verploegen, S. C. B. Mannsfeld, S. Atahan-Evrenk, D. H. Kim, S. Y. Lee, H. A. Becerril, A. Aspuru-Guzik, M. F. Toney and Z. A. Bao, Nature **480** (7378), 504-U124 (2011).